VALUE-BASED DEEP RL SCALES PREDICTABLY

Oleh Rybkin[1] **Michal Nauman**[1,2] **Preston Fu**[1] **Charlie Snell**[1] **Pieter Abbeel**[1] **Sergey Levine**[1] **Aviral Kumar**[3]
[1]University of California, Berkeley [2]University of Warsaw [3]Carnegie Mellon University

ABSTRACT

Scaling data and compute is critical to the success of modern ML. However, scaling demands ***predictability***: we want methods to not only perform well with more compute or data, but also have their performance be predictable from small-scale runs, without running the large-scale experiment. In this paper, we show that value-based off-policy RL methods are predictable despite community lore regarding their pathological behavior. First, we show that data and compute requirements to attain a given performance level lie on a *Pareto frontier*, controlled by the updates-to-data (UTD) ratio. By estimating this frontier, we can predict this data requirement when given more compute, and this compute requirement when given more data. Second, we determine the optimal allocation of a total resource *budget* across data and compute for a given performance and use it to determine hyperparameters that maximize performance for a given budget. Third, this scaling is enabled by first estimating predictable relationships between *hyperparameters*, which is used to manage effects of overfitting and plasticity loss unique to RL. We validate our approach using three algorithms: SAC, BRO, and PQL on DeepMind Control, OpenAI gym, and IsaacGym, when extrapolating to higher levels of data, compute, budget, or performance.

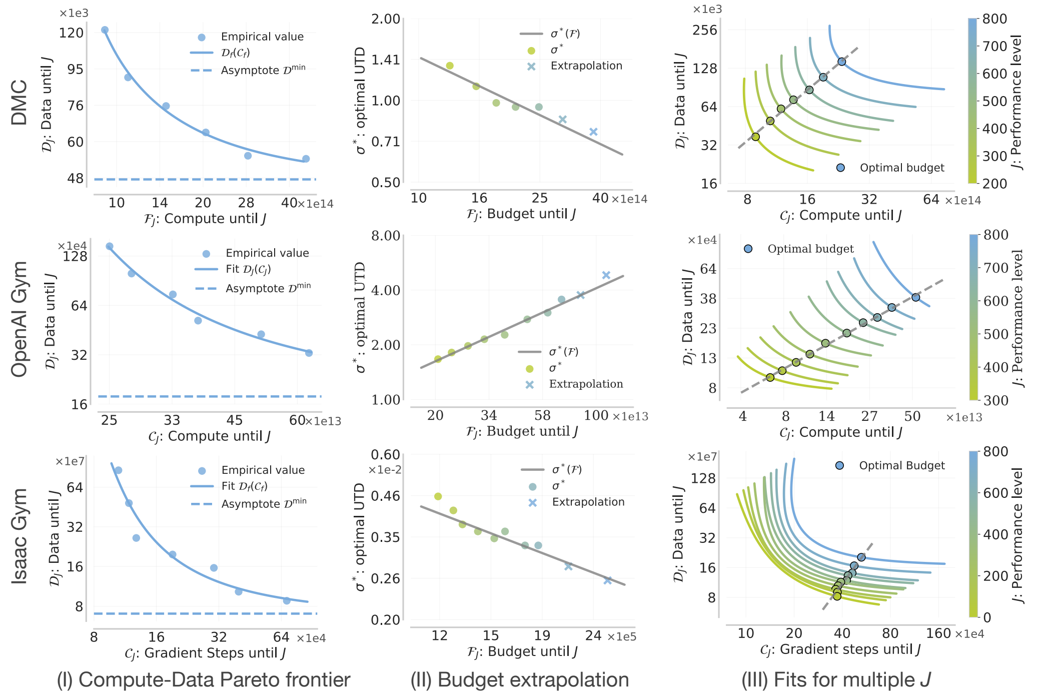

Figure 1: ***Scaling properties when increasing compute $\mathcal{C}$, data $\mathcal{D}$, budget $\mathcal{F}$, or performance J.*** **Left:** Compute versus data requirements Pareto frontier controlled by the UTD ratio σ. We observe that we can trade off data for compute and vice versa, and this relationship is predictable. **Middle:** Extrapolation from low to high performance. We observe that the optimal resource allocation controlled by σ evolves predictably with increasing budget, and can be used to extrapolate from low to high performance. **Right:** Pareto frontiers for several performance levels J.

1 Introduction

Many latest advances in various areas of machine learning have emerged from training big models on large datasets. Successfully executing even one such training run requires a large amount of data, compute, and wall-clock time, such as weeks or months (Achiam et al., 2023; Team et al., 2023). To maximize the success of these large-scale runs, the trend in the machine learning (ML) community has shifted toward not just performant, but also more **predictable algorithms that scale reliably** with more compute and data, such that performance can be predicted from small-scale experiments, without actually running the large-scale experiment. (McCandlish et al., 2018; Kaplan et al., 2020).

In this paper, we study if deep reinforcement learning (RL) is also amenable to such scaling and predictability benefits. We focus on **value-based methods** that train value functions using temporal difference (TD) learning, which are known to be performant at small scales (Mnih et al., 2015; Lillicrap et al., 2015; Haarnoja et al., 2018a). Compared to policy gradient (Mnih, 2016; Schulman et al., 2017) and search methods (Silver et al., 2016), value-based RL can learn from arbitrary data and require less sampling or search, which is inefficient or infeasible when data collection is costly.

We study scaling properties by predicting relationships between different **resources required for training**. *Data* requirement $\mathcal{D}$ is the amount of data needed to attain a certain level of performance. Likewise, *compute* requirement $\mathcal{C}$ refers to the amount of FLOPs or gradient steps needed to attain a certain level of performance. In RL uniquely, performance can be improved by increasing *either* available data or compute (e.g., training multiple times on the same data), which we capture via a *budget* requirement that combines data and compute $\mathcal{F} = \mathcal{C} + \delta \cdot \mathcal{D}$, where δ refers to a constant multiplier. An additive budget function is representative of practical scenarios where the cost of data and compute can be expressed in similar units, such as wall-clock time or required finances.

To establish scaling relationships, we first require a way to predict the **best hyperparameter settings** at each scale. We find that learning rate η, batch size B, and the updates-to-data (UTD) ratio σ are most crucial. While supervised learning benefits from abundant theory to set hyperparameters optimally (Krizhevsky, 2014; McCandlish et al., 2018; Yang et al., 2022), value-based RL often does not satisfy supervised learning assumptions. Specifically, distribution shift due to policy changes (Levine et al., 2020) contributes to a form of overfitting of the value function. In addition, objective shift due to changing target values (Dabney et al., 2020) contributes to "plasticity loss" (D'Oro et al., 2022; Kumar et al., 2021a). We show that it is possible to account for value-based RL training dynamics, and find the best hyperparameters by setting the batch size and learning rate inversely proportional to the UTD ratio. We estimate this dependency using a power law (Kaplan et al., 2020), and observe this model makes effective predictions.

Using the best predicted hyperparameters, we are now able to establish that data and compute requirements evolve as a predictable function of the UTD ratio σ. Furthermore, σ defines the **tradeoff between data and compute**, which can be visualized as a Pareto frontier (Figure 1, left). Using this model, we are able to extrapolate the resource requirements from low-compute to high-compute setting, as well as from low-data to high-data setting as shown in the figure. Using the Pareto frontiers, we are now able to **extrapolate from low to high performance levels**. Instead of extrapolating as a function of return, which can be arbitrary and non-smooth, we extrapolate as a function of the allowed budget $\mathcal{F}$. We can define an optimal tradeoff between data and compute, and we observe that such optimal tradeoff value evolves predictably to higher budgets, which also attains higher performance (Figure 1, middle). Thus we are able to predict optimal hyperparameters, as well as data and compute allocation, for high-budget runs using only data from low-budget runs.

Our contribution is showing that the behavior of value-based deep RL methods based on TD-learning is predictable in larger data and compute regimes. Specifically, we:

1. establish predictable rules for dependencies between batch size (B), learning rate (η), and UTD ratio (σ) in value-based RL, and show that these rules enable more effective scaling.
2. show that data and compute required to attain a given performance level lie on a Pareto frontier, and are respectively predictable in the higher-compute or higher-data regimes.
3. show the optimal allocation of budget between data and compute, and predict how such allocation evolves with higher budgets for best performance.

Our findings apply to algorithms such as SAC, BRO, and PQL, and domains such as the DeepMind Control Suite (DMC), OpenAI Gym, and IsaacGym. The generality of our conclusions challenges conventional wisdom and community lore that value-based deep RL does not scale predictably.

2 RL Preliminaries and Notation

We study standard off-policy online RL, which maximizes the agent's return by training on a replay buffer and periodically collecting new data (Sutton & Barto, 2018). Value-based deep RL methods train a Q-network, Q_θ, to minimize the temporal difference (TD) error:

$$L(\theta) = \mathbb{E}_{(s,a,s')\sim\mathcal{P},a'\sim\pi(\cdot|s')}\left[\left(r(s,a) + \gamma\bar{Q}(s',a') - Q_\theta(s,a)\right)^2\right], \tag{2.1}$$

where $\mathcal{P}$ is the replay buffer, $\bar{Q}$ is the target Q-network, s denotes a state, and a' is an action drawn from a policy $\pi(\cdot|s)$ that aims to maximize $Q_\theta(s,a)$. We implement this operation by sampling a batch of size B from the buffer and taking a gradient step along the gradient of this loss with a learning rate η. In theory, off-policy algorithms can be made very sample efficient by minimizing the TD error fully over any data batch, which in practice translates to making more update steps to the Q-network per environment step, or higher "updates-to-data" ratio (UTD) (Chen et al., 2020). However, increasing the UTD ratio naïvely can lead to worse performance (Nikishin et al., 2022; Janner et al., 2019). To this end, unlike the standard supervised learning or LLM literature that considers B and η as two main hyperparameters affecting training (Kaplan et al., 2020; Hoffmann et al., 2022), our setting presents another hyperparameter, the UTD ratio σ that we also study.

Notation. In this paper, we focus on the following key hyperparameters: the UTD ratio σ, learning rate η, and the batch size B. We will answer questions pertaining to performance of a policy π denoted by $J(\pi)$, the total data utilized by an algorithm to reach a given target level of performance J (denoted by $\mathcal{D}_J$), and the total compute budget utilized by the algorithm to reach performance J (denoted by $\mathcal{C}_J$), which is measured in terms of FLOPs or wall-clock time taken by the algorithm.

3 Problem Statement and Formulation

To demonstrate that the behavior of value-based RL can be predicted reliably at scale, we first post multiple *resource optimization* questions that guide our scaling study. Viewing data and compute as two resources, we answer questions of the form: *what is the minimum value of* `[resource]` *needed to attain a given target performance? And what should the hyperparameters (e.g., B, η, σ) be in such this training run?* We will answer questions of this form by fitting empirical laws from low data and compute runs to determine relationships between hyperparameters. Doing so, in turn, enables us to determine how to set hyperparameters and allocate resources to maximize performance when provided with a larger data and compute budget. Note that we wish to make these hyperparameter predictions without running the large data and compute budget experiment. While questions of this form have been studied in supervised learning, answering them is different in the context of online RL, because online RL requires the algorithm to collect its own data during training, which ties data and compute in a complex manner and breaks i.i.d. nature of datapoints and induces complexities.

Concretely, we study three resource optimization questions: **(1)** maximizing sample efficiency (i.e., minimize the amount of data $\mathcal{D}$ to attain a given target performance under a given compute budget), **(2)** conversely, minimizing compute $\mathcal{C}$ (e.g., FLOPs or gradient steps, whichever is more appropriate for the practitioner) to attain a given performance given an upper bound on data that can be collected, and **(3)** maximizing performance given a total bound on data and compute.

Problem 3.1 (Resource optimization problems)**.** Find the best configuration (B, η, σ) for algorithm Alg that minimizes either the data $\mathcal{D}$ or compute $\mathcal{C}$ consumed to obtain performance J_0:

1. *Maximal sample efficiency*:
$$(B^*, \eta^*, \sigma^*) := \arg\min_{(B,\eta,\sigma)} \quad \mathcal{D} \text{ s.t. } J\left(\pi_{\mathrm{Alg}}(B,\eta,\sigma)\right) \geq J_0,\ \ \mathcal{C} \leq \mathcal{C}_0$$
2. *Maximal compute efficiency*:
$$(B^*, \eta^*, \sigma^*) := \arg\min_{(B,\eta,\sigma)} \quad \mathcal{C} \text{ s.t. } J\left(\pi_{\mathrm{Alg}}(B,\eta,\sigma)\right) \geq J_0,\ \ \mathcal{D} \leq \mathcal{D}_0$$

We solve these problems by fitting empirical models of the minimum data and compute needed to attain a target performance for different values of J_0. Doing so allows us to then solve the third setting **(3)** for maximizing performance given a total budget on data and compute as shown below.

Problem 3.2 (Maximize performance at large data and compute budget)**.** Find the best configuration (B, η, σ) and resource allocations for data $\mathcal{D}$ and compute $\mathcal{C}$ that enable Alg to maximize performance at budget $\mathcal{F}_0$

$$(B^*, \eta^*, \sigma^*) := \arg\max_{(B,\eta,\sigma)} \quad J\left(\pi_{\text{Alg}}(B, \eta, \sigma)\right) \;\text{ s.t. }\; \mathcal{C} + \delta \cdot \mathcal{D} \leq \mathcal{F}_0.$$

4 Scaling Results For Value-Based Deep RL

We will now present our main results addressing Problem 3.1 under the two settings discussed above. We will then use these results to solve Problem 3.2. To do so, we run several experiments and estimate scaling trends from the results. Although this procedure might appear standard from language modeling, we found that instantiating it for value-based RL requires understanding the interaction of the various hyperparameters appearing in TD updates, and the data and compute efficiency of the algorithm. We will formalize these relationships via empirically estimated *laws* and show that these laws extrapolate reliably to new settings not used to obtain these empirical laws. Therefore, in this section, we present empirical and conceptual arguments to build functional forms of relationships between different hyperparameters. Before doing so, we provide our answers to Problems 3.1 and 3.2.

4.1 Main Scaling Results

We begin by answering Problem 3.1 where we maximize sample efficiency. We wish to estimate the minimum amount of data $\mathcal{D}_J$ needed to attain a given performance, given an upper bound on compute $\mathcal{C} \leq \mathcal{C}_0$. To do so, we fit $\mathcal{D}_J$ needed to attain performance J_0 parameterized by the UTD ratio σ (Eq. (4.1)). Intuitively, we would expect the minimum amount of data needed to attain a given performance to be low as more updates are made per datapoint (i.e., when σ is high), as more "value" could be derived from the same datapoint. In addition, we would expect that even for the best value of σ, there is a minimum number of datapoints $\mathcal{D}^{\min}$ that are needed to learn given the "intrinsic" difficulty of the task at hand. Based on these intuitions, we hypothesize a power law relationship between $\mathcal{D}_J(\sigma)$ and σ, with an offset $\mathcal{D}^{\min}$ and constants α_J and β_J.

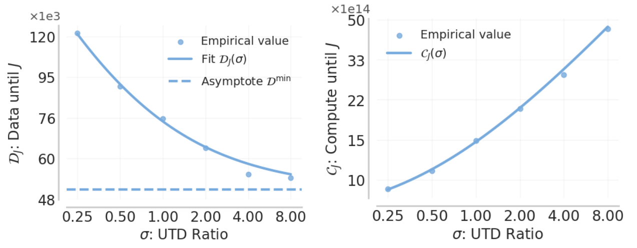

Figure 2: The data-compute tradeoff on DMC. ***Left:*** The minimum required data $\mathcal{D}_J$ scales with the UTD σ as a power law. ***Right:*** The minimum required compute $\mathcal{C}_J$ increases with the UTD σ as a sum of two power laws.

$$\mathcal{D}_J(\sigma) \approx \mathcal{D}_J^{\min} + \left(\frac{\beta_J}{\sigma}\right)^{\alpha_J} \tag{4.1}$$

We validate the efficacy of this fit on DMC in Figure 2. We emphasize this power law is *predictable*, i.e. we can predict $\mathcal{D}_J$ for values of σ that outside the range of σ values used to get the fit (Figure 6).

Scaling Observation 1: Data Requirements

The amount of data $\mathcal{D}_J$ needed to reach a given return target J_0 decreases as a predictable function of the UTD σ, and is a power law (Eq. (4.1)).

To answer the optimization questions in Problem 3.1, we also need an expression for required compute until the target return $\mathcal{C}_J$. As σ determines the number of gradient steps run per data point, $\mathcal{C}_J$ is a function of σ. In particular, total compute is equal to the number of gradient steps taken multiplied by the parameter count of the model. Our study does not optimize over the model size and treats it as a constant. Thus, we can write the compute $\mathcal{C}_J$ as a function of σ as:

$$\mathcal{C}_J(\sigma) \approx 10 \cdot N \cdot B(\sigma) \cdot \sigma \cdot \mathcal{D}_J(\sigma) \tag{4.2}$$

where N denotes the model size, $B(\sigma)$ denotes the "best choice" batch size for a given UTD value σ, and other variables follow definitions from before. Note the additional factor of 10 in Eq. (4.2) emerges from the use of multiple forward passes to compute the loss function for value-based RL and the backward pass, through the Q-network (to contrast with language modeling, the typical multiplier is 6; the gap in our setting comes from the use of multiple forward passes). We plot $\mathcal{C}_J(\sigma)$ for different values of σ and $J = J_0$ in Figure 2. Since $\mathcal{D}_J(\sigma)$ is not a constant and depends itself on σ, we note that this particular relationship between $\mathcal{C}_J(\sigma)$ and σ is not a simple power law unlike Eq. (4.1). Instead, our derivation in Eq. (A.4) shows that $\mathcal{C}_J(\sigma)$ is given by a sum of two different power laws in σ. Similarly to $\mathcal{D}_J$, we also observe that the compute utilized is a *predictable* function of σ: we are able to accurately estimate the compute at larger values of σ using Eq. (4.2).

Scaling Observation 2: Compute Requirements

The compute $\mathcal{C}_J$ to attain a given return target J_0 increases as a predictable function of the UTD ratio σ, and is a sum of two power laws (Eq. (4.2)).

We observe that both required compute and data are controlled by the UTD ratio σ, which allows us to define a tradeoff between compute and data controlled by σ. We plot this tradeoff as a curve with compute $\mathcal{C}_J(\sigma)$ as x-axis and $\mathcal{D}_J(\sigma)$ as y-axis in Figure 1 (left). Further, as $\mathcal{D}_J(\sigma)$ is a monotonically decreasing function of σ, this curve defines a Pareto frontier: we can move left on the curve to increase data efficiency as the expense of compute and move right to increase compute efficiency at the expense of data. Interestingly, due to the compute law being a sum of two power laws, in many environments there is a minimum σ after which compute efficiency no longer improves.

Solving for maximal data efficiency (Problem 3.1, (1)). Our strategy to address setting **(1)** is to find the largest σ (say $\sigma_{\max}$) that satisfies the compute constraint $\mathcal{C}_J(\sigma) \leq \mathcal{C}_0$, and then plug this $\sigma_{\max}$ into $\mathcal{D}_J(\sigma)$ to obtain the data estimate. This enables us to express $\mathcal{D}_J$ directly as a function of the available compute $\mathcal{C}_0$, as we calculate in Eq. (4.2). This can be visualized as finding the value $\mathcal{D}_J$ corresponding to some value $\mathcal{C}_0$ on the Pareto frontier (Figure 1, left)

Solving for maximal compute efficiency (Problem 3.1, (2)). Likewise, the solution can be obtained by finding the smallest value of σ in the range that satisfies the data constraint $\mathcal{D}_J(\sigma) \leq \mathcal{D}_0$, and computing the corresponding value of $\mathcal{C}_J(\sigma)$. This can similarly be visualized on the Pareto frontier (Figure 1, left). We summarize our observations in terms of the following takeaway.

Solving Problem 3.1: Defining the Compute-Data Pareto frontier

The UTD ratio σ defines a Pareto frontier between data and compute requirements, and estimating this frontier yields predictable solutions to resource optimization problems in settings **(1)** and **(2)**. Theoretically, the optimal $\mathcal{D}_J^*$ for an available compute budget $\mathcal{C}_0$ is:

$$\mathcal{D}_J^*(\mathcal{C}_0) \approx \mathcal{C}_0 \cdot (10 \cdot N \cdot B(\sigma^*) \cdot \sigma^*)^{-1}. \tag{4.3}$$

The optimal $\mathcal{C}_J$ for a given data budget $\mathcal{D}_0$ is:

$$\mathcal{C}_J^*(\mathcal{D}_0) \approx 10 \cdot N \cdot B(\sigma^*) \cdot \sigma^* \cdot \mathcal{D}_0. \tag{4.4}$$

Above, σ^* denotes the minimizing UTD value. Calculation details are in Appendix A.

Maximize return within a budget (Problem 3.2). Finally, we tackle Problem 3.2 in order to extrapolate from low to high return. Here, we do not want to minimize resources, but rather want to maximize performance within a given total "budget" on data and compute. As discussed in Section 3, we consider budget functions linear in both data and compute, i.e., $\mathcal{F} = \mathcal{C} + \delta \cdot \mathcal{D}$, for a given constant δ. Our estimated Pareto frontier in Eq. (4.4) will enable answering this question. To do so, we turn to directly predicting a good UTD value σ^*. This UTD value is one that not only leads to maximal performance, but also stays within the total resource budget $\mathcal{F}_0$. Once the UTD value has been identified, it prescribes a concrete way to partition the total resource budget into good data and compute requirements using the solutions to Problem 3.1.

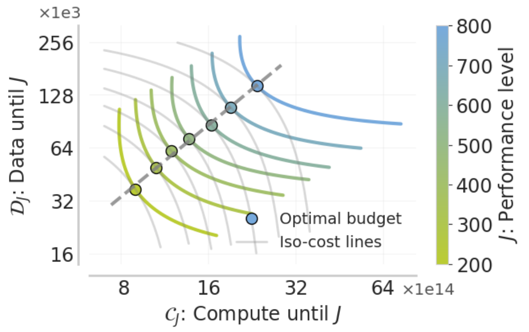

Figure 3: Visualization of the solution to Problem 3.2. Several Pareto frontiers (Figure 1, left) are shown, together with lines of iso-budget $\mathcal{F}$, which define optimal budget points $(\mathcal{D}^*, \mathcal{C}^*)$. Corresponding optimal UTD ratios σ^* are a predictable function of the budgets $\mathcal{F}_0$, trend line shown dashed.

We plot the data-compute Pareto frontiers for multiple values of J_0 in Figure 3 and in Figure 1 (right), and find that these curves move diagonally to the top-right for larger J_0. Intersecting these curves with iso-budget frontiers over $\mathcal{D}$ and $\mathcal{C}$ prescribed by the budget function, gives us the largest possible J_0 for which there is still a $(\mathcal{D}, \mathcal{C})$ pair that just falls just within the budget $\mathcal{F}_0$ but attains performance J_0 (see Figure 3). Since both $\mathcal{D}$ and $\mathcal{C}$ are explained by σ, we can associate this point with a given σ value. Hence, we can estimate the best value of $\sigma^*(\mathcal{F}_0)$ for a given budget threshold $\mathcal{F}_0$. Concretely, we observe a power law between $\sigma(\mathcal{F}_0)$ and $\mathcal{F}_0$, with constants β_σ and α_σ.

$$\sigma^*(\mathcal{F}_0) \approx \left(\frac{\beta_\sigma}{\mathcal{F}_0}\right)^{\alpha_\sigma}. \tag{4.5}$$

Solving Problem 3.2: Maximize return given a total data and compute budget

The best UTD value σ that leads to maximal J is a function of the budget $\mathcal{F}_0$ over data and compute, this relationship follows a power law, and also extrapolates to larger budgets.

This relationship produces the optimal σ, and as a result, the optimal data and compute allocations to reliably attain maximum performance. As shown in Figure 1, estimating this law from low-budget experiments is sufficient for predicting good σ values for large budget runs. These predicted $\sigma^*(\mathcal{F}_0)$ values extrapolate reliably to budgets outside the range used to fit this law.

4.2 Fitting Relationships Between (B, η, σ)

To arrive at these scaling law fits above, we had to set hyperparameters B and η, which we empirically observed to be important. We fit these hyperparameters as a function of σ, the only variable appearing in many of the scaling relationships discussed above. In this section, we will now describe how to estimate good values of B and η in terms of σ. Our analysis here relies crucially on the behavior of TD-learning that is distinct from supervised learning, where the UTD ratio σ does not exist.

To understand relationships between batch size B, learning rate η, and the UTD ratio σ, we ran an extensive grid search. We first attempted to explain the relationship between the B and η values with best data efficiency (denoted B^*, η^*) using tools from supervised learning: *when the batch size is smaller than the critical batch size, B and η are inversely correlated with each other* (McCandlish et al., 2018). However, as shown in Figure 5 (right), we find that best B^* and η^* exhibit weak correlation. Further, the critical batch size (McCandlish et al., 2018) does not correlate with empirically best batch size as we show in Appendix E. Instead, surprisingly, we observe a strong correlation between B^* and σ, as well as η^* and σ, respectively. Since B^* and η^* exhibit near zero correlation among themselves, we can simply omit their dependency and opt for modeling them independently as a function of the UTD ratio, σ. We conceptually explain relationships between B^* and σ, and η^* and σ below and show that models developed from this understanding enable us to reliably predict good values of B and η, allowing us to fully answer Problem 3.1.

Predicting best choice of B in terms of σ. Our proposed functional form for the best batch size B^* takes the form of a power law in σ, which we empirically validate in Figure 5 (left). Intuitively, large batch sizes increase the risk of overfitting because they lead to repetitive training on a fixed set of data. Furthermore, a small training loss on the distribution of data in the buffer does not necessarily reflect the behavior policy distribution of a learning agent (Levine et al., 2020). This means that minimizing the training loss to a large extent can result in poor test performance $J(\pi)$, as also seen by prior work (Li et al., 2023a; Nauman et al., 2024a). One way to counteract this form of "overfitting" from a high UTD value σ is to instead reduce the batch size in the run so that the training process sees a given sample fewer times. In fact, for a fixed UTD value σ, we empirically validate this hypothesis that a lower B leads to substantially reduced overfitting on several tasks in Figure 4. Hence, we post an inverse relationship between the best batch size B^* and the UTD value σ. We show in Figure 5 that indeed this inverse relationship can be estimated well by a power law, given formally as:

$$B^*(\sigma) \approx \left(\frac{\beta_B}{\sigma}\right)^{\alpha_B}. \tag{4.6}$$

Predicting best choice of learning rate η as a function of σ. Next we turn to understanding the relationship between η and σ. We start from a simple observation: a large σ can lead to worse performance not only due to overfitting but also due to plasticity loss (Kumar et al., 2021a; D'Oro

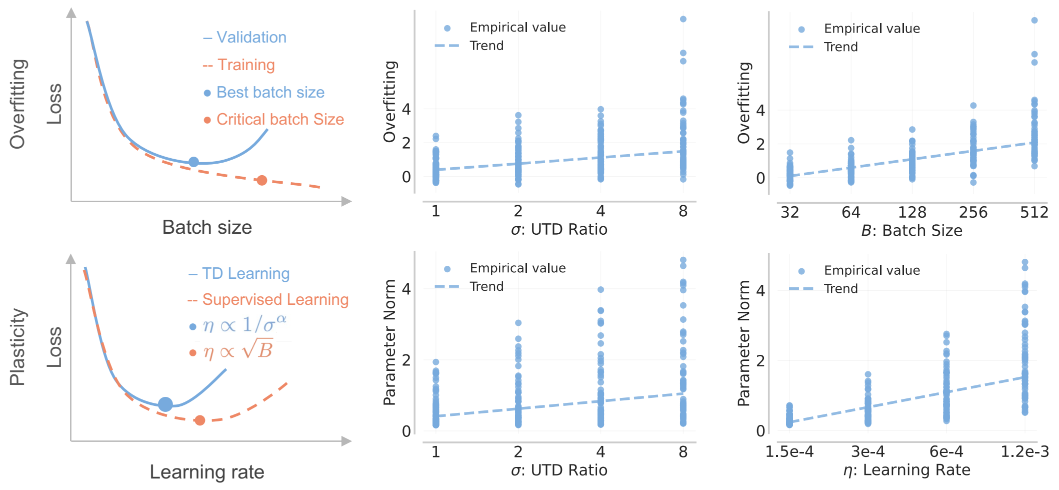

(I) Hparam choice for SL vs RL (II) Effect of UTD ratio σ (III) Effect of B and η

Figure 4: Hyperparameter effects in supervised learning and TD learning on DMC. ***Top:*** Overfitting increases with UTD while batch size can be used to counteract it. ***Bottom:*** Higher UTD leads to poor training dynamics and plasticity loss (D'Oro et al., 2022). Lower learning rates can be used to counteract it. While these relationships are not perfectly predictable, we use them to inform our design choices.

et al., 2022; Lyle et al., 2023), defined broadly as the inability of the value network to fit TD targets appearing later in training. Prior work claims that larger norms of parameters of the Q-network are indicative of plasticity loss (D'Oro et al., 2022; Lyle et al., 2023). We would expect a larger learning rate to make higher magnitude updates against the same TD target, and hence move parameters to a state that suffers from difficulty in fitting subsequent targets (Dabney et al., 2021; Lee et al., 2024). As shown in Figure 4, the parameter norm indeed increases with a high learning rate. Therefore, we hypothesize that the best choice of learning rate, $\eta^*(\sigma)$ should scale inversely in σ. Empirically we observe this is indeed the case (Figure 5 (middle)), and we model this relationship:

$$\eta^*(\sigma) \approx \left(\frac{\beta_\eta}{\sigma}\right)^{\alpha_\eta}. \tag{4.7}$$

Scaling Observation 3: Hyperparameter Selection

The best choices for the batch size and learning rate are predictable functions of the UTD σ, and both of these relationships follow a power law.

4.3 Empirical Workflow for Obtaining Fits

Our Workflow for Fitting Empirical Relationships

1. Run a sweep for batch size B and learning rate η for several values of UTD σ. Since the batch size and learning rate are independent for the best σ, we can run these sweeps independently.
2. Estimate empirically the best of batch size $\tilde{B}$ and learning rate $\tilde{\eta}$, with statistical bootstrapping.
3. Fit $B^*(\sigma)$ and $\eta^*(\sigma)$ on $\tilde{B}$, $\tilde{\eta}$ according to Equations (4.6) and (4.7).
4. Using the found fits $B^*(\sigma), \eta^*(\sigma)$, run different values of σ that cover a range spanning an order of magnitude; we use $16\times$, i.e., $\sigma_{\text{max}}/\sigma_{\text{min}} > 16$.
5. Fit $\mathcal{D}_J(\sigma)$ according to Eq. (4.1).
6. Using fits of $\mathcal{D}_J(\sigma)$ for different values of J_0, fit $\sigma^*(\mathcal{F}_0)$ according to Eq. (4.5).
7. Optimal hyperparameters can now be extrapolated to larger data, larger compute, or larger budget settings according to Problem 3.1.

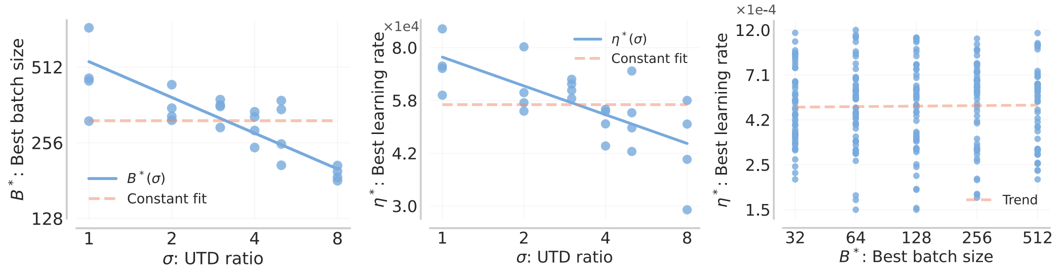

Figure 5: ***Left, middle***: Fitting the best learning rate η^* and batch size B^* given UTD σ on DMC. Modeling the dependency on σ is crucial to obtain good hyperparameters, whereas using constant B, η as is commonly done leads too poor extrapolation. ***Right:*** the best learning rate and batch size are not significantly correlated, a major difference from supervised learning.

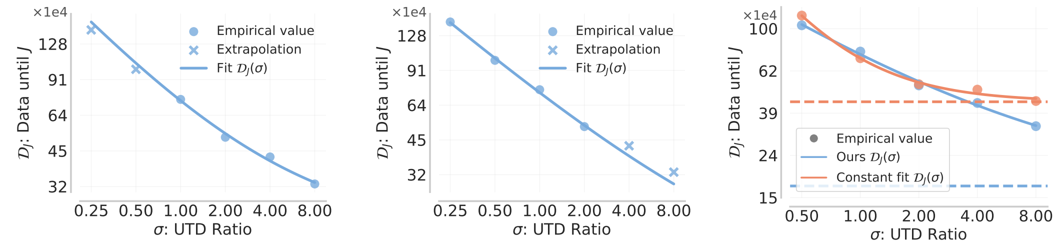

Figure 6: Extrapolation towards unseen values of σ on OpenAI Gym. **Left:** We show Pareto frontier extrapolation towards higher data regime. **Middle:** We show Pareto frontier extrapolation towards higher compute regime. **Right:** We compare the best-performing hyperparameters (red) for $\sigma = 2$ to hyperparameters predicted via our proposed workflow (blue).

Having presented solutions to Problems 3.1 and 3.2, we now present the workflow we utilize to estimate these empirical fits. Further details are in Section 5 and Appendix D. This workflow can serve as a useful skeletion for scaling law studies with other value-based algorithms as well.

4.4 Evaluating Extrapolation

Evaluating budget extrapolation. Results on all environments are shown in Figure 1 (middle). We estimate several Pareto frontiers corresponding to points with equal changes in budget. We perform the $\sigma^*(\mathcal{F}_0)$ fit, while holding out two largest budgets. The quality of our fit for these two extrapolated budgets can be seen in the figure.

Evaluating Pareto frontier extrapolation. Results on OpenAI Gym are shown in Figure 6. We fit the data efficiency equation $\mathcal{D}_J(\sigma)$ Eq. (4.1) while holding out either two UTD values σ with largest data requirement (left) or two σ values with largest compute requirement (right). The quality of our fit for these two extrapolated σ values can be seen in the figure.

Hyperparameter fit extrapolation. Results on OpenAI Gym are shown in Figure 6 (right). We plot the data efficiency fit when using hyperparameters according to our found dependency $B^*(\sigma), \eta^*(\sigma)$ (shown in olive). These fits are estimated from $\sigma = 1, \cdots, 8$ and extrapolated to $\sigma = 0.5$. We compare to the typical approach to tuning hyperparameters, where hyperparameters are tuned for one setting of $\sigma = 2$ and this setting is used for all UTD values (shown in blue). We see that our proposed hyperparameter fits improve results for values other than $\sigma = 2$. Further, this improvement is larger for larger values of σ, showing that accounting for hyperparameter dependency is critical.

5 Experimental Details

Experimental Setup We focus on 12 tasks from 3 domains in our study. On **OpenAI Gym** (Brockman et al., 2016), we use Soft Actor Critic, a commonly used TD-learning algorithm (Haarnoja et al., 2018b). We first run a sweep on 5 values of η, then a grid of runs with 4 values of σ and 3 values of B, and then use hyperparameter fits to run 2 more value of σ with 8 seeds per task. To test our approach with larger models, we use **DMC** (Tassa et al., 2018), where, we utilize the state-of-the-art Bigger, Regularized, Optimistic (BRO) algorithm (Nauman et al., 2024b) that uses a larger and more modern architecture. We first run 5 values of B, 4 values of η, and 4 σ; and then use hyperparameters fits to run 2 more values of σ, with 10 seeds per task. Finally, we test our approach with more data on

IsaacGym (Makoviychuk et al., 2021), where we use the Parallel Q-Learning (PQL) algorithm (Li et al., 2023b), which was designed to leverage massively parallel simulation like Isaac Gym that can quickly produce billions of environment samples. Because of computational expense, we only run one IsaacGym task. We first run 4 values of σ, 3 values of η, as well as 5 values of B, with 5 seeds per task, after which we run a second round of grid search with 7 values of σ. Further details are in Appendices B and D and Table 3.

Fitting Functional Forms for Scaling Laws We approximate Eq. (4.1) via brute-force search followed by LBFG-S with a log-MSE loss following (Hoffmann et al., 2022). For Equations (4.6) and (4.7), we fit a line in log space using least squares regression following Kaplan et al. (2020). In our experiments, we run a single fit that is shared across different tasks in a given benchmark. Specifically, we share the slope α_B, α_η and use task-specific intercepts $\sigma_B^{\text{env}}, \sigma_\eta^{\text{env}}$ (as defined in Equations (4.6) and (4.7)) to be different for separate tasks. This technique is standard in ordinary least squares modeling and is referred to as fixed effect regression (Bishop & Nasrabadi, 2006). Sharing this slope serves the goal of variance reduction, which can be important if the granularity of the grid search over various hyperparameters run is coarse. More details are in Appendices B and D.

6 Related Work

Scaling laws and predictability. Prior work has studied scaling laws in the context of supervised learning (Kaplan et al., 2020; Hoffmann et al., 2022), primarily to predict the effect of model size and training data on validation loss, while marginalizing out hyperparameters like batch size (McCandlish et al., 2018) and learning rate (Kaplan et al., 2020). There are several extensions of such scaling laws for language models, such as laws for settings with data repetition (Muennighoff et al., 2023) or mixture-of-experts (Ludziejewski et al., 2024), but most focus on cross-entropy loss, with an exception of Gadre et al. (2024), which focuses on downstream metrics. While scaling laws have guided supervised learning experiments, little work explores this for RL. The closest works are: Hilton et al. (2023) which fits power laws for on-policy RL methods using model size and the number of environment steps; Jones (2021) which studies the scaling of AlphaZero on board games of increasing complexity; and Gao et al. (2023) which studies reward model overoptimization in RLHF. In contrast, we are the first ones to study off-policy value-based RL methods that are trained via TD-learning. Not only do off-policy methods exhibit training dynamics distinct from supervised learning and on-policy methods (Kumar et al., 2021b; Lyle et al., 2023), but we show that this distinction also results in a different functional form for scaling law altogether.

Methods for large-scale deep RL. Recent work has scaled deep RL across three axes: model size (Kumar et al., 2023; Schwarzer et al., 2023; Nauman et al., 2024b), data (Kumar et al., 2023; Gallici et al., 2024; Singla et al., 2024), and UTD (Chen et al., 2020; D'Oro et al., 2022). Naïve scaling of model size or UTD often degrades performance or causes divergence (Nikishin et al., 2022; Schwarzer et al., 2023), mitigated by classification losses (Kumar et al., 2023), layer normalization (Nauman et al., 2024a), or feature normalization (Kumar et al., 2021b). In on-policy RL, prior works focus on effective learning from parallelized data streams in a simulator or a world model (Mnih, 2016; Silver et al., 2016; Schrittwieser et al., 2020). Follow-up works like IMPALA (Espeholt et al., 2018) and SAPG (Singla et al., 2024) use a centralized learner that collects experience from distributed workers with importance sampling updates. These works differ substantially from our study as we focus exclusively on value-based off-policy RL algorithms that use TD-learning and not on-policy methods. In value-based RL, prior work on data scaling focuses on offline (Yu et al.; Kumar et al., 2023; Park et al., 2024) and multi-task RL (Hafner et al., 2023). In contrast, we study online RL and fit scaling laws to answer resource optimization questions.

7 Conclusion

In this paper, we show that value-based deep RL algorithms scale predictably. We establish relationships between good values of hyperparameters of value-based RL. We then establish a relationship between required data and required compute for a certain performance. Finally, this allows us to determine an optimal allocation of resources to either data and compute. Although only estimated from small-scale runs, our empirical models reliably *extrapolate* to large compute, data, budget, or performance regimes. To the best of our knowledge, this is the first demonstration that it is possible to predict behavior of value-based off-policy RL algorithms at larger scale using small-scale runs.

REFERENCES

Josh Achiam, Steven Adler, Sandhini Agarwal, Lama Ahmad, Ilge Akkaya, Florencia Leoni Aleman, Diogo Almeida, Janko Altenschmidt, Sam Altman, Shyamal Anadkat, et al. Gpt-4 technical report. *arXiv preprint arXiv:2303.08774*, 2023.

Richard E Barlow and Hugh D Brunk. The isotonic regression problem and its dual. *Journal of the American Statistical Association*, 67(337):140–147, 1972.

Christopher M Bishop and Nasser M Nasrabadi. *Pattern recognition and machine learning*, volume 4. Springer, 2006.

Greg Brockman, Vicki Cheung, Ludwig Pettersson, Jonas Schneider, John Schulman, Jie Tang, and Wojciech Zaremba. Openai gym, 2016.

Xinyue Chen, Che Wang, Zijian Zhou, and Keith W Ross. Randomized ensembled double q-learning: Learning fast without a model. In *International Conference on Learning Representations*, 2020.

Will Dabney, André Barreto, Mark Rowland, Robert Dadashi, John Quan, Marc G Bellemare, and David Silver. The value-improvement path: Towards better representations for reinforcement learning. *arXiv preprint arXiv:2006.02243*, 2020.

Will Dabney, André Barreto, Mark Rowland, Robert Dadashi, John Quan, Marc G Bellemare, and David Silver. The value-improvement path: Towards better representations for reinforcement learning. In *Proceedings of the AAAI Conference on Artificial Intelligence*, volume 35, pp. 7160–7168, 2021.

Pierluca D'Oro, Max Schwarzer, Evgenii Nikishin, Pierre-Luc Bacon, Marc G Bellemare, and Aaron Courville. Sample-efficient reinforcement learning by breaking the replay ratio barrier. In *The Eleventh International Conference on Learning Representations*, 2022.

Lasse Espeholt, Hubert Soyer, Remi Munos, Karen Simonyan, Volodymir Mnih, Tom Ward, Yotam Doron, Vlad Firoiu, Tim Harley, Iain Dunning, et al. Impala: Scalable distributed deep-rl with importance weighted actor-learner architectures. *arXiv preprint arXiv:1802.01561*, 2018.

Samir Yitzhak Gadre, Georgios Smyrnis, Vaishaal Shankar, Suchin Gururangan, Mitchell Wortsman, Rulin Shao, Jean Mercat, Alex Fang, Jeffrey Li, Sedrick Keh, et al. Language models scale reliably with over-training and on downstream tasks. *arXiv preprint arXiv:2403.08540*, 2024.

Matteo Gallici, Mattie Fellows, Benjamin Ellis, Bartomeu Pou, Ivan Masmitja, Jakob Nicolaus Foerster, and Mario Martin. Simplifying deep temporal difference learning. *arXiv preprint arXiv:2407.04811*, 2024.

Leo Gao, John Schulman, and Jacob Hilton. Scaling laws for reward model overoptimization. In *International Conference on Machine Learning*, pp. 10835–10866. PMLR, 2023.

T. Haarnoja, A. Zhou, P. Abbeel, and S. Levine. Soft actor-critic: Off-policy maximum entropy deep reinforcement learning with a stochastic actor. In *arXiv*, 2018a. URL https://arxiv.org/pdf/1801.01290.pdf.

Tuomas Haarnoja, Aurick Zhou, Pieter Abbeel, and Sergey Levine. Soft actor-critic: Off-policy maximum entropy deep reinforcement learning with a stochastic actor. In *International conference on machine learning*, pp. 1861–1870. PMLR, 2018b.

Danijar Hafner, Jurgis Pasukonis, Jimmy Ba, and Timothy Lillicrap. Mastering diverse domains through world models. *arXiv preprint arXiv:2301.04104*, 2023.

Jacob Hilton, Jie Tang, and John Schulman. Scaling laws for single-agent reinforcement learning. *arXiv preprint arXiv:2301.13442*, 2023.

Jordan Hoffmann, Sebastian Borgeaud, Arthur Mensch, Elena Buchatskaya, Trevor Cai, Eliza Rutherford, Diego de Las Casas, Lisa Anne Hendricks, Johannes Welbl, Aidan Clark, et al. Training compute-optimal large language models. *arXiv preprint arXiv:2203.15556*, 2022.

Michael Janner, Justin Fu, Marvin Zhang, and Sergey Levine. When to trust your model: Model-based policy optimization. In *Advances in Neural Information Processing Systems*, pp. 12498–12509, 2019.

Andy L. Jones. Scaling scaling laws with board games, 2021. URL https://arxiv.org/abs/2104.03113.

Jared Kaplan, Sam McCandlish, Tom Henighan, Tom B Brown, Benjamin Chess, Rewon Child, Scott Gray, Alec Radford, Jeffrey Wu, and Dario Amodei. Scaling laws for neural language models. *arXiv preprint arXiv:2001.08361*, 2020.

Alex Krizhevsky. One weird trick for parallelizing convolutional neural networks. *arXiv preprint arXiv:1404.5997*, 2014.

Aviral Kumar, Rishabh Agarwal, Dibya Ghosh, and Sergey Levine. Implicit under-parameterization inhibits data-efficient deep reinforcement learning. In *International Conference on Learning Representations*, 2021a. URL https://openreview.net/forum?id=O9bnihsFfXU.

Aviral Kumar, Rishabh Agarwal, Tengyu Ma, Aaron Courville, George Tucker, and Sergey Levine. DR3: Value-Based Deep Reinforcement Learning Requires Explicit Regularization. *arXiv preprint arXiv:2112.04716*, 2021b.

Aviral Kumar, Rishabh Agarwal, Xinyang Geng, George Tucker, and Sergey Levine. Offline q-learning on diverse multi-task data both scales and generalizes. In *The Eleventh International Conference on Learning Representations*, 2023. URL https://openreview.net/forum?id=4-k7kUavAj.

Hojoon Lee, Hanseul Cho, Hyunseung Kim, Daehoon Gwak, Joonkee Kim, Jaegul Choo, Se-Young Yun, and Chulhee Yun. Plastic: Improving input and label plasticity for sample efficient reinforcement learning. *Advances in Neural Information Processing Systems*, 36, 2024.

Sergey Levine, Aviral Kumar, George Tucker, and Justin Fu. Offline reinforcement learning: Tutorial, review, and perspectives on open problems. *arXiv preprint arXiv:2005.01643*, 2020.

Qiyang Li, Aviral Kumar, Ilya Kostrikov, and Sergey Levine. Efficient deep reinforcement learning requires regulating overfitting. In *The Eleventh International Conference on Learning Representations*, 2023a. URL https://openreview.net/forum?id=14-kr46GvP-.

Zechu Li, Tao Chen, Zhang-Wei Hong, Anurag Ajay, and Pulkit Agrawal. Parallel q-learning: Scaling off-policy reinforcement learning under massively parallel simulation. In *International Conference on Machine Learning*, pp. 19440–19459. PMLR, 2023b.

Timothy P Lillicrap, Jonathan J Hunt, Alexander Pritzel, Nicolas Heess, Tom Erez, Yuval Tassa, David Silver, and Daan Wierstra. Continuous control with deep reinforcement learning. *arXiv preprint arXiv:1509.02971*, 2015.

Jan Ludziejewski, Jakub Krajewski, Kamil Adamczewski, Maciej Pióro, Michał Krutul, Szymon Antoniak, Kamil Ciebiera, Krystian Król, Tomasz Odrzygóźdź, Piotr Sankowski, et al. Scaling laws for fine-grained mixture of experts. In *Forty-first International Conference on Machine Learning*, 2024.

Clare Lyle, Zeyu Zheng, Evgenii Nikishin, Bernardo Avila Pires, Razvan Pascanu, and Will Dabney. Understanding plasticity in neural networks. In *International Conference on Machine Learning*, pp. 23190–23211. PMLR, 2023.

Viktor Makoviychuk, Lukasz Wawrzyniak, Yunrong Guo, Michelle Lu, Kier Storey, Miles Macklin, David Hoeller, Nikita Rudin, Arthur Allshire, Ankur Handa, et al. Isaac gym: High performance gpu-based physics simulation for robot learning. *arXiv preprint arXiv:2108.10470*, 2021.

Sam McCandlish, Jared Kaplan, Dario Amodei, and OpenAI Dota Team. An empirical model of large-batch training. *arXiv preprint arXiv:1812.06162*, 2018.

Volodymyr Mnih. Asynchronous methods for deep reinforcement learning. *arXiv preprint arXiv:1602.01783*, 2016.

Volodymyr Mnih, Koray Kavukcuoglu, David Silver, Andrei A Rusu, Joel Veness, Marc G Bellemare, Alex Graves, Martin Riedmiller, Andreas K Fidjeland, Georg Ostrovski, et al. Human-level control through deep reinforcement learning. *nature*, 518(7540):529–533, 2015.

Niklas Muennighoff, Alexander Rush, Boaz Barak, Teven Le Scao, Nouamane Tazi, Aleksandra Piktus, Sampo Pyysalo, Thomas Wolf, and Colin A Raffel. Scaling data-constrained language models. *Advances in Neural Information Processing Systems*, 36:50358–50376, 2023.

Michal Nauman, Michał Bortkiewicz, Piotr Miłoś, Tomasz Trzcinski, Mateusz Ostaszewski, and Marek Cygan. Overestimation, overfitting, and plasticity in actor-critic: the bitter lesson of reinforcement learning. In *Proceedings of the 41st International Conference on Machine Learning*, 2024a. URL https://arxiv.org/pdf/2403.00514. PMLR 235:37342-37364.

Michal Nauman, Mateusz Ostaszewski, Krzysztof Jankowski, Piotr Miłoś, and Marek Cygan. Bigger, regularized, optimistic: scaling for compute and sample-efficient continuous control. *arXiv preprint arXiv:2405.16158*, 2024b.

Evgenii Nikishin, Max Schwarzer, Pierluca D'Oro, Pierre-Luc Bacon, and Aaron Courville. The primacy bias in deep reinforcement learning. In *International conference on machine learning*, pp. 16828–16847. PMLR, 2022.

Seohong Park, Kevin Frans, Sergey Levine, and Aviral Kumar. Is value learning really the main bottleneck in offline rl? *arXiv preprint arXiv:2406.09329*, 2024.

Julian Schrittwieser, Ioannis Antonoglou, Thomas Hubert, Karen Simonyan, Laurent Sifre, Simon Schmitt, Arthur Guez, Edward Lockhart, Demis Hassabis, Thore Graepel, et al. Mastering atari, go, chess and shogi by planning with a learned model. *Nature*, 588(7839):604–609, 2020.

John Schulman, Filip Wolski, Prafulla Dhariwal, Alec Radford, and Oleg Klimov. Proximal policy optimization algorithms. *arXiv preprint arXiv:1707.06347*, 2017.

Max Schwarzer, Johan Samir Obando Ceron, Aaron Courville, Marc G Bellemare, Rishabh Agarwal, and Pablo Samuel Castro. Bigger, better, faster: Human-level atari with human-level efficiency. In *International Conference on Machine Learning*, pp. 30365–30380. PMLR, 2023.

David Silver, Aja Huang, Chris J Maddison, Arthur Guez, Laurent Sifre, George Van Den Driessche, Julian Schrittwieser, Ioannis Antonoglou, Veda Panneershelvam, Marc Lanctot, et al. Mastering the game of go with deep neural networks and tree search. *nature*, 529(7587):484–489, 2016.

Jayesh Singla, Ananye Agarwal, and Deepak Pathak. Sapg: split and aggregate policy gradients. *arXiv preprint arXiv:2407.20230*, 2024.

Richard S Sutton and Andrew G Barto. *Reinforcement learning: An introduction*. MIT press, 2018.

Yuval Tassa, Yotam Doron, Alistair Muldal, Tom Erez, Yazhe Li, Diego de Las Casas, David Budden, Abbas Abdolmaleki, Josh Merel, Andrew Lefrancq, et al. Deepmind control suite. *arXiv preprint arXiv:1801.00690*, 2018.

Gemini Team, Rohan Anil, Sebastian Borgeaud, Jean-Baptiste Alayrac, Jiahui Yu, Radu Soricut, Johan Schalkwyk, Andrew M Dai, Anja Hauth, Katie Millican, et al. Gemini: a family of highly capable multimodal models. *arXiv preprint arXiv:2312.11805*, 2023.

Saran Tunyasuvunakool, Alistair Muldal, Yotam Doron, Siqi Liu, Steven Bohez, Josh Merel, Tom Erez, Timothy Lillicrap, Nicolas Heess, and Yuval Tassa. dm_control: Software and tasks for continuous control. *Software Impacts*, 6:100022, 2020. ISSN 2665-9638. doi: https://doi.org/10.1016/j.simpa.2020.100022. URL https://www.sciencedirect.com/science/article/pii/S2665963820300099.

Pauli Virtanen, Ralf Gommers, Travis E Oliphant, Matt Haberland, Tyler Reddy, David Cournapeau, Evgeni Burovski, Pearu Peterson, Warren Weckesser, Jonathan Bright, et al. Scipy 1.0: fundamental algorithms for scientific computing in python. *Nature methods*, 17(3):261–272, 2020.

Greg Yang, Edward J Hu, Igor Babuschkin, Szymon Sidor, Xiaodong Liu, David Farhi, Nick Ryder, Jakub Pachocki, Weizhu Chen, and Jianfeng Gao. Tensor programs v: Tuning large neural networks via zero-shot hyperparameter transfer. *arXiv preprint arXiv:2203.03466*, 2022.

T. Yu, A. Kumar, et al. How to Leverage Unlabeled Data in Offline Reinforcement Learning. *ICML 2022*.

Appendices

A Additional details on derivations

FLOPs calculation. Recall that FLOPs per forward and backward passes are equal to $\mathcal{C}_J^{\text{forward}}(\sigma) \approx 2 \cdot N \cdot B(\sigma) \cdot \sigma \cdot \mathcal{D}_J(\sigma)$ and $\mathcal{C}_J^{\text{backward}}(\sigma) \approx 4 \cdot N \cdot B(\sigma) \cdot \sigma \cdot \mathcal{D}_J(\sigma)$, with σ denoting the number of gradient steps per environment steps. Q-learning methods used in our study use MLP and ResNet architectures, which are well modeled with this approximation. Assuming same size for actor and critic as an approximation, a training iteration of the critic requires three forward passes and one backward pass, totaling $\mathcal{C}_J^{\text{critic}}(\sigma) \approx 10 \cdot N \cdot B(\sigma) \cdot \sigma \cdot \mathcal{D}_J(\sigma)$. A training iteration of the actor requires two forward and two backward passes, totaling $\mathcal{C}_J^{\text{actor}}(\sigma) \approx 12 \cdot N \cdot B(\sigma) \cdot \sigma \cdot \mathcal{D}_J(\sigma)$. Here we follow the standard practice of updating the actor every time a new data point collected, while the critic is updated according to the UTD ratio σ. Since we expect the critic to be updated more then the actor. As such, in this study we assume

$$\mathcal{C}_J(\sigma) \approx \mathcal{C}_J^{\text{critic}}(\sigma) \approx 10 \cdot N \cdot B(\sigma) \cdot \sigma \cdot \mathcal{D}_J(\sigma). \tag{A.1}$$

Compute and sample efficiency. Following Eq. (4.1), the number of data points required to achieve performance J is equal to:

$$\mathcal{D}_J(\sigma) \approx \mathcal{D}_J^{\min} + \left(\frac{\beta_J}{\sigma}\right)^{\alpha_J} \tag{A.2}$$

Given the expressions for required data points, practical batch size, and FLOPs Equations (4.1), (4.6) and (A.1), we can now derive the expression for compute required to reach a particular performance expressed in terms of σ. First, note that the number of parameter updates is

$$\sigma \cdot \mathcal{D}_J(\sigma) \approx \sigma \cdot \mathcal{D}_J^{\min} + \frac{\beta_J^{\alpha_J}}{\sigma^{\alpha_J - 1}} \tag{A.3}$$

Combining above, Eq. (4.6) with Eq. (A.1) yields:

$$\begin{aligned}
\mathcal{C}_J(\sigma) &\approx 10 \cdot N \cdot B(\sigma) \cdot \left(\sigma \cdot \mathcal{D}_J^{\min} + \frac{\beta_J^{\alpha_J}}{\sigma^{\alpha_J - 1}}\right) \\
&\approx 10 \cdot N \cdot \left(\frac{\beta_B}{\sigma}\right)^{\alpha_B} \cdot \left(\sigma \cdot \mathcal{D}_J^{\min} + \frac{\beta_J^{\alpha_J}}{\sigma^{\alpha_J - 1}}\right) \\
&\approx 10 \cdot N \cdot \left(\frac{\mathcal{D}_J^{\min} \cdot \beta_B^{\alpha_B}}{\sigma^{\alpha_B - 1}} + \frac{\beta_J^{\alpha_J} \cdot \beta_B^{\alpha_B}}{\sigma^{\alpha_J + \alpha_B - 1}}\right).
\end{aligned} \tag{A.4}$$

We observe that the resulting expression is a sum of two power laws. In practice, one of the power laws will dominate the expression and a simple mental model is that compute increases with UTD as a power law with a coefficient < 1 (see Figure 2).

Maximal compute efficiency. Here, we solve the compute optimization problem presented in Section 3. We write the problem:

$$(B^*, \eta^*, \sigma^*) := \arg\min_{(B,\eta,\sigma)} \; \mathcal{C} \quad \text{s.t.} \quad J\left(\pi_{\text{Alg}}(B, \eta, \sigma)\right) \geq J_0 \quad \wedge \quad \mathcal{D} \leq D_0. \tag{A.5}$$

Firstly, we formulate the Lagrangian $\mathcal{L}$:

$$\begin{aligned}
\mathcal{L}(\sigma, \lambda) &= \mathcal{C}_J(\sigma) + \lambda \cdot (\mathcal{D}_J(\sigma) - D_0) \\
&\approx 10 \cdot N \cdot B(\sigma) \cdot \left(\sigma \cdot \mathcal{D}_J^{\min} + \frac{\beta_J^{\alpha_J}}{\sigma^{\alpha_J - 1}}\right) + \lambda \cdot \left(\mathcal{D}_J^{\min} + \left(\frac{\beta_J}{\sigma}\right)^{\alpha_J} - \mathcal{D}_0\right)
\end{aligned} \tag{A.6}$$

Here, the constrained with respect to performance J_0 is upheld through the use of $\mathcal{C}_J(\sigma)$ and $\mathcal{D}_J(\sigma)$ which are defined such that $J = J_0$. We proceed with calculating the derivative with respect to λ to find the minimal σ that is able to achieve the desired sample efficiency $\mathcal{D}_J$. We denote such such optimal UTD as σ^*:

$$\frac{\partial \mathcal{L}}{\partial \lambda} = \mathcal{D}_J^{\min} + \left(\frac{\beta_J}{\sigma}\right)^{\alpha_J} - \mathcal{D}_0 = 0 \quad \Longrightarrow \quad \sigma^* = \frac{-\beta_J}{\left(\mathcal{D}_J^{\min} - \mathcal{D}_0\right)^{1/\alpha_J}} \tag{A.7}$$

Then, we substitute the σ^* into the expression defining compute, as well as use Eq. (4.6):

$$\begin{aligned} \mathcal{C}_J(\sigma^*) &\approx 10 \cdot N \cdot \frac{\beta_B^{\alpha_B}}{\sigma^{\alpha_B - 1}} \cdot \left(\mathcal{D}_J^{\min} + \frac{\beta_J^{\alpha_J}}{\sigma^{\alpha_J}}\right) \\ &\approx 10 \cdot N \cdot \frac{\beta_B^{\alpha_B}}{(\sigma^*)^{\alpha_B - 1}} \cdot \left(\mathcal{D}_J^{\min} + \frac{\beta_J^{\alpha_J} \cdot \left(\mathcal{D}_J^{\min} - \mathcal{D}_0\right)}{-\beta_J^{\alpha_J}}\right) \\ &\approx 10 \cdot N \cdot \beta_B^{\alpha_B} \cdot (\sigma^*)^{1-\alpha_B} \cdot \mathcal{D}_0 \end{aligned} \tag{A.8}$$

Maximal sample efficiency. Firstly, we note that we treat $B(\sigma)$ as a constant and do not optimize with respect to it. We start with the problem definition:

$$(B^*, \eta^*, \sigma^*) := \arg\min_{(B,\eta,\sigma)} \quad \mathcal{D} \quad \text{s.t.} \quad J\left(\pi_{\text{Alg}}(B, \eta, \sigma)\right) \geq J_0 \quad \wedge \quad \mathcal{C} \leq C_0. \tag{A.9}$$

Similarly to the maximal compute efficiency problem, we formulate the Lagrangian $\mathcal{L}$:

$$\begin{aligned} \mathcal{L}(\sigma, \lambda) &= \mathcal{D}_J(\sigma) + \lambda \cdot (\mathcal{C}_J(\sigma) - C_0) \\ &\approx \mathcal{D}_J^{\min} + \left(\frac{\beta_J}{\sigma}\right)^{\alpha_J} + \lambda \cdot \left(10 \cdot N \cdot B(\sigma) \cdot \sigma \cdot \left(\mathcal{D}_J^{\min} + \frac{\beta_J^{\alpha_J}}{\sigma^{\alpha_J}}\right) - \mathcal{C}_0\right) \end{aligned} \tag{A.10}$$

Again, we uphold the constraint with respect to the performance through the use of $\mathcal{D}_J(\sigma)$ and $\mathcal{C}_J(\sigma)$. We calculate the derivative with respect to λ:

$$\frac{\partial \mathcal{L}}{\partial \lambda} = 10 \cdot N \cdot B(\sigma) \cdot \sigma \cdot \left(\mathcal{D}_J^{\min} + \frac{\beta_J^{\alpha_J}}{\sigma^{\alpha_J}}\right) - \mathcal{C}_0 = 0 \quad \Longrightarrow \quad \mathcal{D}_J^{\min} + \frac{\beta_J^{\alpha_J}}{\sigma^{\alpha_J}} = \frac{\mathcal{C}_0}{10 \cdot N \cdot B(\sigma) \cdot \sigma} = \mathcal{D}_J \tag{A.11}$$

Since $\mathcal{D}_J$ is monotonic in σ and does not model impact of B on the sample efficiency, the optimization problem can be solved via Weierstrass extreme value theorem. As such, we find the biggest σ and that fulfills the compute constraint, and find the data requirement for such σ.

B Experimental details

For our experiments, we use a total of 12 tasks from 3 benchmarks (DeepMind Control (Tunyasuvunakool et al., 2020), Isaac Gym (Makoviychuk et al., 2021), and OpenAI Gym (Brockman et al., 2016)). We list all considered tasks in Table 1.

Figure 1. We use all available UTD values for the fits, which is 6 for DMC, 5 for OAI Gym, and 7 for Isaac Gym. Given the dependency of compute and data on UTD, we plot the resulting curve. We average the data efficiencies across all tasks in each domain, as described in Appendix D.

We calculate compute given the model sizes of $N = 4.92\text{e}6$ for DMC, $N = 1.5\text{e}5$ for OAI Gym, and $N = 2\text{e}6$ following standard implementations of the respective algorithms.

Table 1: Tasks used in presented experiments.

Domain	Task	Optimal π Returns
DeepMind Control	Cartpole-Swingup	1000
	Cheetah-Run	1000
	Dog-Stand	1000
	Finger-Spin	1000
	Humanoid-Stand	1000
	Quadruped-Walk	1000
	Walker-Walk	1000
Isaac Gym	Franka-Push	0.05
OpenAI Gym	HalfCheetah-v4	8500
	Walker2d-v4	4500
	Ant-v4	6625
	Humanoid-v4	6125

For budget extrapolation, we use tradeoff values δ to mimic the wall-clock time of the algorithm. We use $\delta = 1\text{e}10$ for DMC, $\delta = 5\text{e}9$ for OAI Gym, and $\delta = 1\text{e}4$ for Isaac Gym. We exclude runs affected by resets ($\sigma = 8$) for DMC since the returns right after the reset are lower, which adds noise to the results.

Figure 2. We use the same data as for DMC in Figure 1 (left).

Figure 3. We use the same data as for DMC in Figure 1 (right).

Figure 5. In the left and central Figures, we evaluate the B^* and η^* models. For each DMC task, we find the best hyperparameters according to our workflow and procedure described in Section 5 and Appendix D. While the intercepts vary across environments, for simplicity we plot data points and fits from all environments in the same figure by shifting them with the corresponding intercept. In the right Figure, we marginalize over σ and visualize best performing pairs of B and η.

Figure 4. **Left**: we show an illustration that reflects our observed empirical results about the dependencies between hyperparameters.

Right, middle: we investigate the correlations between overfitting, parameter norm of the critic network, and σ. We observed the same relationships on all tasks. Here, to avoid clutter, we plot 3 tasks from DMC benchmark: cheetah-run, dog-stand, and quadruped-walk. To measure overfitting, we compare the TD loss calculated on samples randomly sampled from the buffer (corresponding to *training data*) to TD loss calculated on 16 newest transitions (corresponding to *validation data*) according to:

$$\text{Overfitting} = TD^{\text{training}} - TD^{\text{validation}}. \tag{B.1}$$

We fit the linear curves using ordinary least squares with mean absolute error loss.

Figure 6. Here, we investigate 4 tasks from OpenAI Gym, listed in Table 1, and compare the extrapolation performance of two hyperparameter sets: the best performing hyperparameters for $\sigma = 1$, found by testing 8 different hyperparameter values listed in Table 3 (we refer to this configuration as *baseline*); and hyperparameters predicted by our proposed models of B^* and η^*. We fit our models using $\sigma \in (1, 2, 4, 8)$, and extrapolate to $\sigma \in (0.5, 16)$. The graph shows the data efficiency with threshold as 700, normalized according to the procedure in Appendix D.

Figure 7. The goal of the left Figure is to visualize the effects of isotropic regression fit on a noisy data. We use the SciPy package (Virtanen et al., 2020) to run the isotropic model. In the right Figure we visualize the process of best hyperparameter selection using bootstrapped confidence intervals. We describe the bootstrapping strategy in Appendix D.

C Resulting Fits

DMC Refer to Table 2 for environment-specific values.

$$\begin{aligned}
\eta^* &= \beta_\eta \cdot \sigma^{-0.26} \\
B^* &= \beta_B \cdot \sigma^{-0.47} \\
\mathcal{D}_J &= \mathcal{D}^{\text{min}} \cdot \left(1 + \left(\frac{\sigma}{0.45}\right)^{-0.74}\right) \\
\sigma^* &= 1.4\text{e}8 \cdot \mathcal{F}_0^{-0.53}
\end{aligned} \tag{C.1}$$

OpenAI Gym Refer to Table 2 for environment-specific values.

$$\begin{aligned}
\eta^* &= \beta_\eta \sigma^{-0.30} \\
B^* &= \beta_B \sigma^{-0.33} \\
\mathcal{D}_J &= \mathcal{D}^{\text{min}} \cdot \left(1 + \left(\frac{\sigma}{4.02}\right)^{-0.69}\right) \\
\sigma^* &= 1.4\text{e}8 \cdot \mathcal{F}_0^{-0.53}
\end{aligned} \tag{C.2}$$

Isaac Gym

$$\begin{aligned}
\eta^* &= 8.77 \cdot \left(1 + \left(\frac{\sigma}{2.57\text{e-}3}\right)^{-0.26}\right) \\
B^* &= 38.6 \cdot \left(1 + \left(\frac{\sigma}{1.42\text{e-}2}\right)^{-0.68}\right) \\
\mathcal{D}_J &= 6.8\text{e}7 \cdot \left(1 + \left(\frac{\sigma}{1.88}\right)^{-0.87}\right) \\
\sigma^* &= 11.3 \cdot \mathcal{F}_0^{-0.57}
\end{aligned} \tag{C.3}$$

Table 2: Coefficients for DMC and OpenAI Gym fits.

Domain	**Task**	β_η	β_B	$\mathcal{D}^{\text{min}}$
DMC	cartpole-swingup	7.55e-4	538.2	2.4e4
	cheetah-run	6.25e-4	564.9	3.5e5
	finger-spin	8.77e-4	608.2	2.9e4
	humanoid-stand	3.86e-4	451.8	3.8e5
	quadruped-walk	8.46e-4	526.4	6.2e4
	walker-walk	9.38e-4	313.3	3.3e4
OpenAI Gym	Ant-v4	1.35e-4	447.0	2.7e5
	HalfCheetah-v4	1.86e-3	415.4	7.8e4
	Humanoid-v4	1.65e-4	351.6	1.8e5
	Walker2d-v4	7.85e-4	399.1	1.7e5

Table 3: Tested configurations.

Hyperparameters	**DeepMind Control**	**Isaac Gym**	**OpenAI Gym**
Updates-to-data σ	1, 2, 4, 8	$\frac{1}{1024}, \frac{1}{2048}, \frac{1}{4096}, \frac{1}{8192}, \frac{1}{16384}, \frac{1}{32768}, \frac{1}{65536}$	1, 2, 4, 8
Batch size B	32, 64, 128, 256, 512	512, 1024, 2048, 4096, 8192	128, 256, 512
Learning rate η	15e-5, 3e-4, 6e-4, 12e-3	1e-4, 2e-4, 3e-4	1e-4, 2e-4, 5e-4, 1e-3, 2e-3

D Additional details on the fitting procedure

Preprocessing return values. In order to estimate the fits from our laws, we need to track the data and compute needed by a run to hit a target performance level. Due to stochasticity both in training and and evaluation, naïve measurements of this point can exhibit high variance. This in turn would result in low-quality fits for $\mathcal{D}_J$ and $\mathcal{C}_J$. Thus, we preprocess the return values before estimating the fits by running isotonic regression (Barlow & Brunk, 1972). Isotonic regression transforms return values to the most aligned monotonic sequence of values that can then be used to estimate $\mathcal{D}_J$. While in general return values can decrease with more training after reaching a target value, and this will result in a large deviation between the isotonic fit and true return values, the proposed isotonic transformation still suffices for us as our goal is to simply fit the *minimum* number of samples or compute needed to attain a target return. As we can still make reliable predictions that extrapolate to larger scales, the downstream impact of this error is clearly not substantial. We also average across random seeds before running isotonic regression to further reduce noise. We normalize the returns for all environments to be between 0 and 1000 (Table 1 lists pre-normalized returns), and reserve the points of 700 and 800 for budget extrapolation in Figure 1.

Uncertainty-adjusted optimal hyperparameters. While averaging across seeds and applying isotonic regression reduces noise, we observe that the granularity of our grid search on learning rate and batch size limits the precision of the resulting hyperparameter fits $\tilde{B}$, $\tilde{\eta}$. Noise due to random seed generation makes hyperparameter selection harder as some hyperparameters that appear empirically optimal might simply be so due to noise. We observe that we can correct for this precision loss by constructing a more precise estimate of $\tilde{B}$, $\tilde{\eta}$ adjusted for this uncertainty. Specifically, we run $K = 100$ bootstrap estimates by sampling n random seeds with replacement out of the original n random seeds, applying isotonic regression, and selecting the optimal hyperparameters $\tilde{B}_k$, $\tilde{\eta}_k$. We then use the mean of this bootstrapped estimate to improve the precision:

$$\begin{aligned} \tilde{B}_{\text{bootstrap}} &= \frac{1}{K}\sum_k \tilde{B}_k \\ \tilde{\eta}_{\text{bootstrap}} &= \frac{1}{K}\sum_k \tilde{\eta}_k \end{aligned} \tag{D.1}$$

We have also experimented with more precise laws for learning rate and batchsize by adding an additive offset. In this case, we follow Hoffmann et al. (2022) and fit the data using brute-force search followed by LBFG-S. We use MSE in log space as the error: $\text{MSE}_{\log}(a, b) = (\log a - \log b)^2$.

$$B^*(\sigma) \approx B_{\text{min}} + \frac{\sigma_B}{\sigma^{\alpha_B}} \tag{D.2}$$

$$\eta^*(\sigma) \approx \eta_{\text{min}} + \frac{\sigma_\eta}{\sigma^{\alpha_\eta}}. \tag{D.3}$$

However, we found that this more complex fit did not validate the decrease of degrees of freedom given a limited sweep range, resulting in accuracy of extrapolation.

Independence of B and η. Whereas the optimal choice of B and η is often intertwined as UTD changes, we observe in our experiments that the correlation between them is relatively low (Figure 5). If we ran a cross-product grid search with hyperparameter space $\{B_1, \ldots, B_{n_B}\} \times \{\eta_1, \ldots, \eta_{n_\eta}\}$, we can use this fact to further improve the results by averaging the estimate $\tilde{B}$ over different values of η. That is, we produce the estimate $\tilde{B}^{[\eta=\eta_i]}$ (respectively $\tilde{\eta}^{[B=B_i]}$) by only looking at the runs where $\eta = \eta_i$, and averaging such estimates.

$$\begin{aligned} \tilde{B}_{\text{mean}} &= \frac{1}{n_\eta}\sum_i \tilde{B}^{[\eta=\eta_i]} \\ \tilde{\eta}_{\text{mean}} &= \frac{1}{n_B}\sum_i \tilde{\eta}^{[B=B_i]} \end{aligned} \tag{D.4}$$

Data efficiency. We fit data efficiency of the runs with our found practical hyperparameters B^*, η^* according to Eq. (4.1). We follow Hoffmann et al. (2022) and fit the data using brute-force search followed by LBFG-S. We use MSE in log space as the error: $\text{MSE}_{\log}(a, b) = (\log a - \log b)^2$.

In DeepMind Control Suite, we would like to share the data efficiency fit across different environments env. We normalize the data efficiency $\mathcal{D}$ by the intra-environment median data efficiency medians

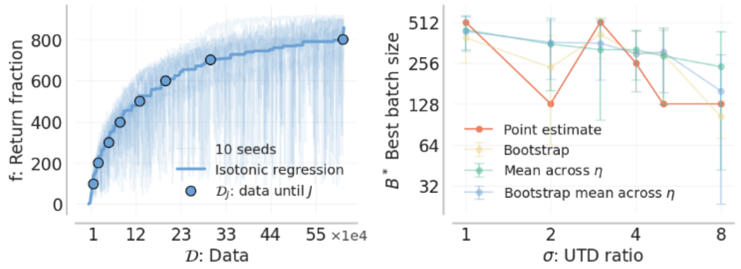

Figure 7: ***Left:*** Determining performance via isotonic regression on DMC. ***Right:*** improving hyperparameter selection with uncertainty adjustment on DMC. Further details are in Appendix D.

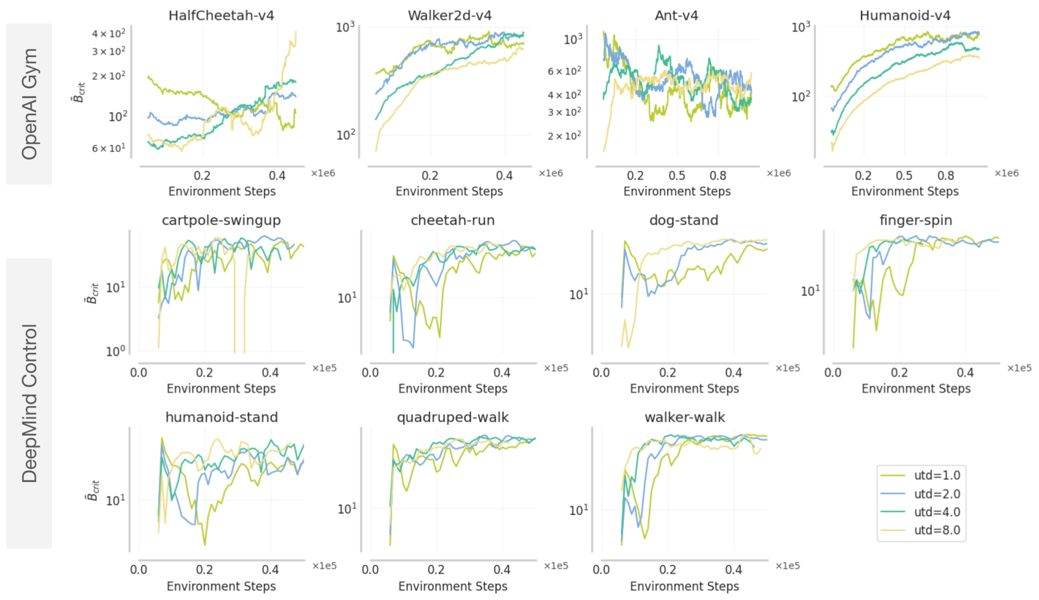

Figure 8: An approximation of the critical batch size over training. Further details are in Appendix E.

$\mathcal{D}^{\text{env}}_{\text{med}} = \text{median}\{\mathcal{D}^{\text{env}}_{[\sigma=\sigma_i]} | i = 1..n_\sigma\}$. For interpretability, we further re-normalize D with the overall median $\mathcal{D}_{\text{med}}$: $\mathcal{D}_{\text{norm}} = \mathcal{D} \cdot \mathcal{D}_{\text{med}} / \mathcal{D}^{\text{env}}_{\text{med}}$. We will need to express the data efficiency law alternatively as:

$$D_J(\sigma) \approx \mathcal{D}^{\text{min}}_J \left(1 + \left(\frac{\beta_J}{\sigma}\right)^{\alpha_J}\right). \tag{D.5}$$

This is equivalent to Eq. (4.1) because the coefficient β_J absorbs $\mathcal{D}^{\text{min}}_J$. However, this expression makes explicit an overall multiplicative offset[1] $\mathcal{D}^{\text{min}}_J$. Our median normalization is then equivalent to fitting per-environment coefficients $\mathcal{D}^{\text{min}}_J$, following our procedure for environment-shared hyperparameter fits. However, we further improve robustness by fixing the per-environment coefficients to be the median data efficiency and do not require fitting them.

E CRITICAL BATCH SIZE ANALYSIS

Previous work has argued that there is a critical batch size B_{crit} for neural network training in image classification, generative modeling, and reinforcement learning with policy gradient algorithms (McCandlish et al., 2018) — a transition point at which increasing the batch size begins to yield diminishing returns. We follow this work and compute an estimate of the gradient noise scale $B_{\text{noise}} \approx B_{\text{crit}}$ according to the following procedure: throughout training, we compute the gradient

[1]This form enforces that $\mathcal{D}^{\text{min}}_J$ is positive.

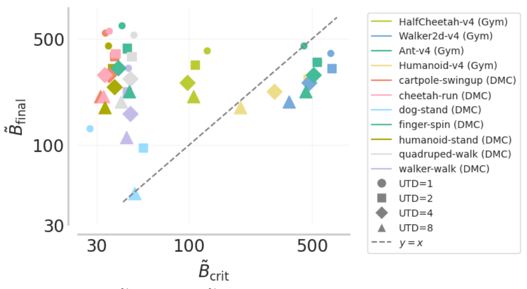

Figure 9: $\tilde{B}_{\text{final}}$ vs. $\tilde{B}_{\text{crit}}$, grouped by task and UTD.

norm $|G_B|$ of the critic network for batches of size $B = B_{\text{small}} := 64$ and $B = B_{\text{big}} := 1024$. Then, we evaluate

$$|\mathcal{G}|^2 := \frac{1}{B_{\text{big}} - B_{\text{small}}} \left(B_{\text{big}} |G_{B_{\text{big}}}|^2 - B_{\text{small}} |G_{B_{\text{small}}}|^2 \right)$$
$$\mathcal{S} := \frac{1}{1/B_{\text{small}} - 1/B_{\text{big}}} \left(|G_{B_{\text{small}}}|^2 - |G_{B_{\text{big}}}|^2 \right)$$

and take $\tilde{B}_{\text{crit}} := \mathcal{S}/|\mathcal{G}|^2$. In practice, to account for the noisiness of $|G|^2$, we first take rolling averages of $|G_{B_{\text{small}}}|$ and $|G_{B_{\text{big}}}|$ over training, and tune the window size so that the estimates for $|\mathcal{G}|^2$ and $\mathcal{S}$ are stable.

We show the values of $\tilde{B}_{\text{crit}}$ over training in Figure 8. Unlike policy gradient methods, we find that the critical batch size (averaged over training) has little correlation with the optimal batch size, as shown in Figure 9.

Table 4: Batch size values predicted by the proposed model on DMC.

Task	$\sigma = 0.25$	$\sigma = 0.5$	$\sigma = 1$	$\sigma = 2$	$\sigma = 4$	$\sigma = 8$
cartpole-swingup	1040	752	544	384	288	208
cheetah-run	1088	784	560	400	288	208
dog-stand	240	176	128	96	64	48
finger-spin	1168	848	608	432	320	224
humanoid-stand	864	624	448	320	240	176
quadruped-walk	1008	736	528	384	272	192
walker-walk	608	432	320	224	160	112

Table 5: Learning rate values predicted by the proposed model on DMC.

Task	$\sigma = 0.25$	$\sigma = 0.5$	$\sigma = 1$	$\sigma = 2$	$\sigma = 4$	$\sigma = 8$
cartpole-swingup	.00108	.000902	.000755	.000631	.000528	.000442
cheetah-run	.000893	.000747	.000625	.000523	.000438	.000366
dog-stand	.000664	.000555	.000465	.000389	.000325	.000272
finger-spin	.00125	.00105	.000877	.000734	.000614	.000514
humanoid-stand	.000551	.000461	.000386	.000323	.00027	.000226
quadruped-walk	.00121	.00101	.000846	.000708	.000592	.000496
walker-walk	.00134	.00112	.000938	.000785	.000657	.000549

Table 6: Batch size values predicted by the proposed model on OpenAI Gym.

Task	$\sigma = 0.25$	$\sigma = 0.5$	$\sigma = 1$	$\sigma = 2$	$\sigma = 4$	$\sigma = 8$	$\sigma = 16$
Ant-v4	704	560	448	352	288	224	176
HalfCheetah-v4	672	528	416	336	256	208	160
Humanoid-v4	560	432	352	272	224	176	144
Walker2d-v4	640	496	400	320	256	192	160

Table 7: Learning rate values predicted by the proposed model on OpenAI Gym.

Task	$\sigma = 0.25$	$\sigma = 0.5$	$\sigma = 1$	$\sigma = 2$	$\sigma = 4$	$\sigma = 8$	$\sigma = 16$
Ant-v4	.000206	.000167	.000138	.000109	.000087	.000070	.000060
HalfCheetah-v4	.002820	.002280	.001900	.001510	.001210	.000972	.000827
Humanoid-v4	.000251	.000203	.000169	.000134	.000107	.000086	.000073
Walker2d-v4	.001180	.000958	.000806	.000640	.000512	.000412	.000347